AD-A063 133 NAVAL RESEARCH LAB WASHINGTON D C F/G 11/6
A CORRELATION BETWEEN SCC PATH, HARDNESS, MICROSTRUCTURE, AND M--ETC(U)
DEC 78 F W FRASER, E A METZBOWER, J STOOP
UNCLASSIFIED NRL-8193 NL

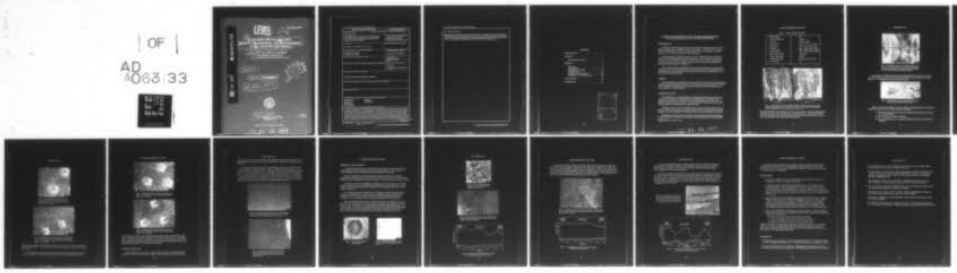

END
DATE FILMED
3-79
DDC

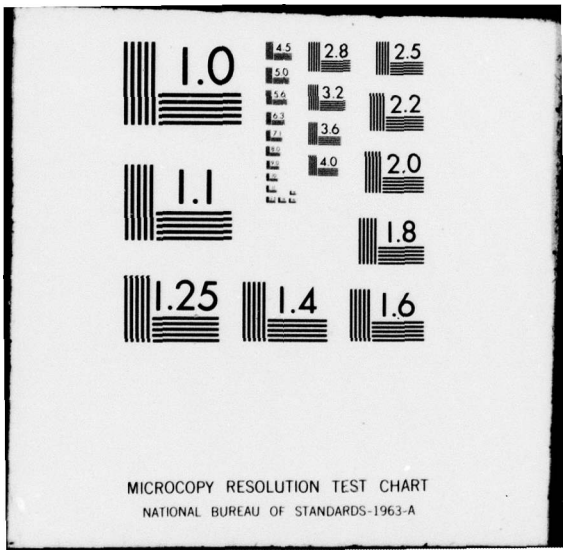
1.0
1.1
1.25
1.4
1.6
1.8
2.0
2.2
2.5
2.8
3.2
3.6
4.0
4.5
5.0
5.6
6.3
MICROCOPY RESOLUTION TEST CHART
NATIONAL BUREAU OF STANDARDS-1963-A

LEVEL II

NRL Report 8193

A Correlation Between SCC Path, Hardness, Microstructure, and Microsegregation in HY-130 E14018 Weld Metal

F. W. FRASER, E. A. METZBOWER AND J. STOOP

Advanced Materials Technology Branch
Material and Radiation Science and Technology Directorate

12 21 p.

11 22 December 1978

14 NRL-8193

NAVAL RESEARCH LABORATORY
Washington, D.C.

SECURITY CLASSIFICATION OF THIS PAGE *(When Data Entered)*

REPORT DOCUMENTATION PAGE		READ INSTRUCTIONS BEFORE COMPLETING FORM
1. REPORT NUMBER NRL Report 8193 ✓	2. GOVT ACCESSION NO.	3. RECIPIENT'S CATALOG NUMBER
4. TITLE *(and Subtitle)* A CORRELATION BETWEEN SCC PATH, HARDNESS, MICROSTRUCTURE, AND MICROSEGREGATION IN HY-130 E14018 WELD METAL		5. TYPE OF REPORT & PERIOD COVERED Final Report on one phase of continuing NRL problem
		6. PERFORMING ORG. REPORT NUMBER
7. AUTHOR(s) F.W. Fraser, E.A. Metzbower, and J. Stoop		8. CONTRACT OR GRANT NUMBER(s)
9. PERFORMING ORGANIZATION NAME AND ADDRESS Naval Research Laboratory Washington, D.C. 20375		10. PROGRAM ELEMENT, PROJECT, TASK AREA & WORK UNIT NUMBERS NRL Problem No. 63M03-05
11. CONTROLLING OFFICE NAME AND ADDRESS		12. REPORT DATE December 22, 1978
		13. NUMBER OF PAGES 20
14. MONITORING AGENCY NAME & ADDRESS*(if different from Controlling Office)*		15. SECURITY CLASS. *(of this report)* Unclassified
		15a. DECLASSIFICATION/DOWNGRADING SCHEDULE

16. DISTRIBUTION STATEMENT *(of this Report)*

Approved for public release; distribution unlimited.

17. DISTRIBUTION STATEMENT *(of the abstract entered in Block 20, if different from Report)*

18. SUPPLEMENTARY NOTES

19. KEY WORDS *(Continue on reverse side if necessary and identify by block number)*

Stress corrosion
Weld metal
Microstructure
Microsegregation
Hardness
Fractography

20. ABSTRACT *(Continue on reverse side if necessary and identify by block number)*

In an investigation of cold cracking in the weld metal of an HY-130 E14018 weldment, variations in hardness, microstructure, and microsegregation were related to the path of the fracture which propagated through the centers of adjacent weld beads. Evidence of solute rejection was found in the formation of pools of solute, in the cell boundaries, where a transition from a cellular to a cellular-dendritic solidification mode had taken place. The composition of the solute pools was determined by microprobe analysis. Microhardness measurements showed a gradient within each weld bead, with hardness increasing from the fracture edge to the fusion zone at the interface of the weld metal and the base metal.

(Continued)

DD FORM 1 JAN 73 1473 EDITION OF 1 NOV 65 IS OBSOLETE
S/N 0102-LF-014-6601

SECURITY CLASSIFICATION OF THIS PAGE *(When Data Entered)*

20. Abstract (Continued)

Metallographic examination showed the microstructure at the fracture edge to be largely bainitic, whereas the harder weld metal, near the fusion zone, was predominantly martensitic. Measurements within the fusion zone showed a slight decrease in hardness, and microprobe analysis showed this to be a zone of melted but incompletely mixed base metal and weld filler metal.

CONTENTS

A CORRELATION BETWEEN SCC PATH, HARDNESS, MICROSTRUCTURE, AND MICROSEGREGATION IN HY-130 E14018 WELD METAL

INTRODUCTION

Variations in hardness, indicating lack of uniformity in strength, can lead to the formation of areas within a weldment that are crack-sensitive. Such areas occur in hard structures, which may not be able to deform sufficiently to accommodate the residual strains, and in soft structures, where yielding takes place.

Crack propagation in weldments cannot, however, be attributed only to variations in hardness. Mixed microstructures, particularly ferrite in a matrix of martensite or bainite, have been found to be highly susceptible to embrittlement and cracking. Embrittlement may also be caused by the concentration of residual elements in grain boundaries and by localized stresses resulting from welding [1].

Also, metallic inclusions, originating from the electrode covering and entrapped in the weld metal, have been shown to give rise to microcracks; furthermore, light etching streaks appearing in the weld metal microstructure have been attributed to the segregation of one or more of the alloying elements [2].

PURPOSE

This investigation was undertaken to relate the location of a crack which had propagated through successive weld beads in a double-V, shielded metal arc (SMA) weldment of HY-130 steel, to variations in hardness and microstructure within each successive bead, and to the microsegregation of alloying elements.

Experimental Procedure

The mating halves of a single edge-notch, cantilever-beam specimen, which had been fractured under stress in a corroding medium, were utilized in this investigation (Fig. 1). This specimen was fabricated as a double-V, SMA (E14018) weldment of HY-130 steel. Welding parameters are given in Table 1. The specimen had been tested for stress corrosion, electrochemically, while galvanically coupled to zinc [3].

The areas of sections A and B, outlined in Fig. 1, depict the analyzed portions of the specimen which encompassed the mid-thickness region, or root, of the weldment, thereby supplying a specimen comprised of weld metal, fusion zone, and heat-affected zone (HAZ).

Fractographic studies of section A, along the edge of stress corrosion cracking (SCC) initiation (arrows), were carried out with the aid of a scanning electron microscope (SEM).

Manuscript submitted August 18, 1978.

Table 1 — SMA Welding Conditions

Weld position	flat
Weld configuration	double - V
Electrode	McKay 14018
Electrode size	diam. - 1/8 in. (3.18 mm)
Equipment	300 - A Lincoln rectifier
Preheat temp.	200° - 300°F (93° - 199°C)
Interpass temp.	275° -300°F (135°-199°C)
Weld current range	120-125 A
Weld voltage range	22-24 V
Average heat input	50 kJ/in. (19.7 kJ/cm)
No. of passes	66

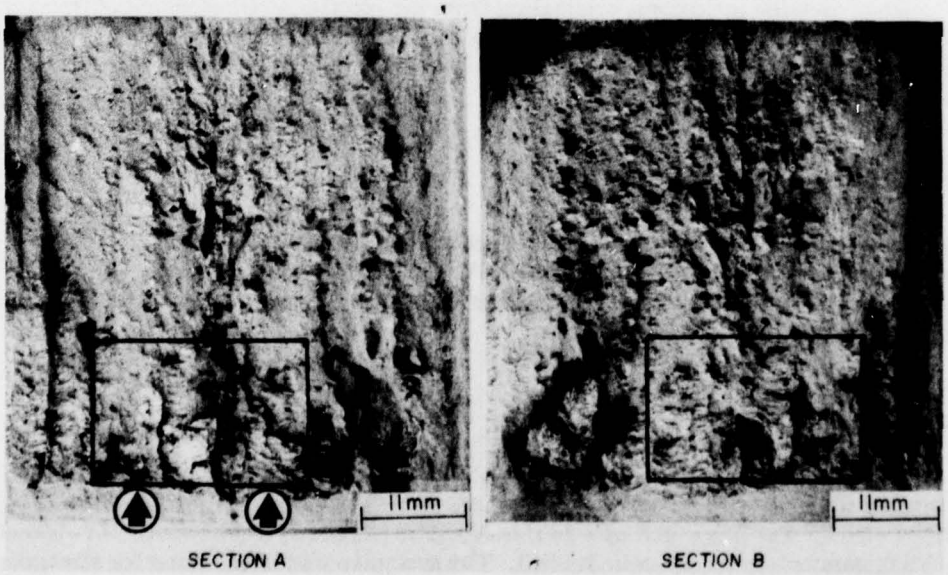

Fig. 1 — Mating halves of HY-130 weldment fractured during stress corrosion testing. Outlined areas indicate portions of specimen analyzed. The arrows indicate edge along which fractographic studies were carried out on section A.

The transverse faces of both sections A and B, at this location, were then polished simultaneously and etched with 10% ammonium persulfate solution. This etchant revealed weld bead placement and the fusion zones, both between weld beads, as seen in Fig. 2, and at the interface of the weld metal and base metal.

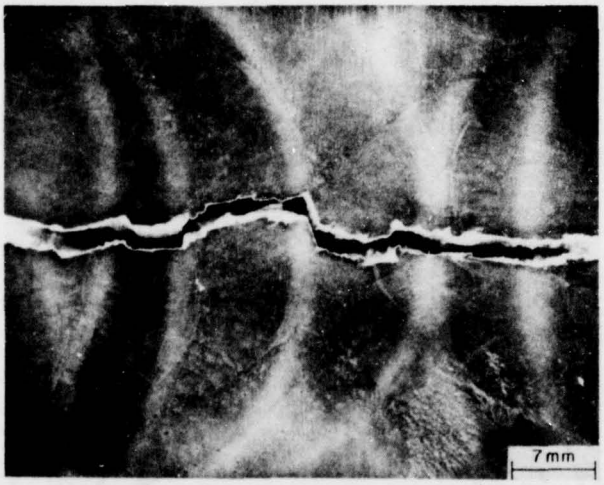

Fig. 2 — Dark field micrograph of transverse, polished cross section of mated sections A (lower) and B (upper) showing weld bead placement and fusion zones between weld beads (etched with 10% ammonium persulfate solution)

The ammonium persulfate etchant also revealed solidification substructure. Section A was subsequently repolished and etched with 1% Nital to reveal structure and relative grain size. A macrograph of section A is shown in Fig. 3.

Fig. 3 — Macrograph of section A showing structure and relative grain size (etched with 1% Nital)

Figure 4 is a schematic diagram of section A (Fig. 3), delineating areas of the weldment discussed throughout the text. These include the following:

(1) The fracture edge, which is seen as the irregular upper boundary of the specimen in the illustration;

(2) The individual weld beads 1 through 6;

(3) The columnar grain zone (C) and the thermally cycled zone (T) within each weld bead;

(4) The fusion boundary between weld beads and at the weld metal-base metal interface indicated by the solid line;

(5) The inverted V of base metal at the center of the weldment, seen in the lower portion of the illustration.

Beads 2, 3, 4, and 5 encompass both columnar grain zones and thermally cycled zones of the weld metal, whereas beads 1 and 6 comprise columnar grain zones only.

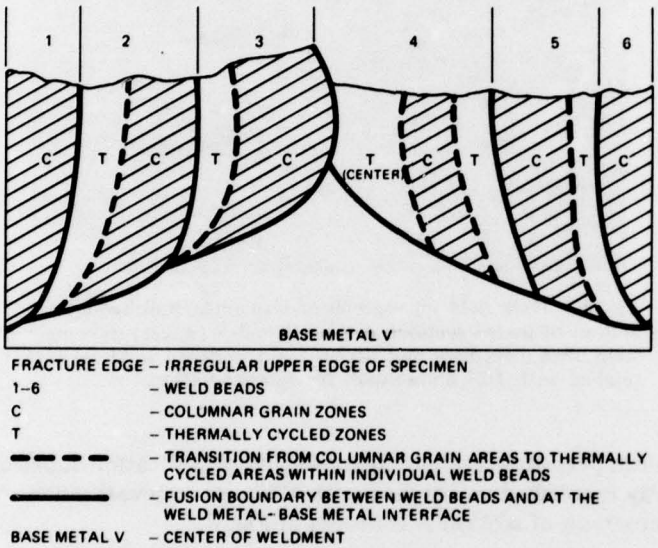

Fig. 4 — Schematic diagram of polished cross section A delineating areas of the weldment discussed throughout the text

By means of a Vickers Microhardness Tester with a 300-G load, hardness measurements were made at intervals through each bead in section A, starting at the fracture edge and progressing longitudinally to the fusion zone at the interface of the weld metal and the base metal. Measurements were made in both the columnar grain zone and the thermally cycled zone of each weld bead.

Additional hardness measurements were made at the fusion boundaries between beads 2 and 3 and between beads 3 and 4. Measurements were continued into the light arcs in the base metal (Fig. 2). All measurements were converted to Rockwell C (Rc) hardness scale.

To investigate variations in composition and the segregation of the major alloying elements Ni, Cr, Mn, and Mo, electron beam microprobe analyses were carried out in selected areas of the fusion zones, both between adjacent weld beads and at the weld metal-base metal interface. Microprobe traces were also made in selected areas at the fracture edges of both sections A and B. The microanalyzer was operated at 25 kV and 0.1 μa. The traces were were made with the electron beam in point mode while the specimen was moved at a constant

speed beneath the stationary beam. Prior to the analysis, the specimen surface was polished and very lightly etched with 10 percent ammonium persulfate solution for orientation purposes.

RESULTS

Grain Size

As depicted in Figs. 3 and 4, the portion of the weldment examined encompassed six weld beads. With the exception of bead 4, at the center of the weldment, the thermally cycled regions near the edge of the fracture consisted primarily of fragmented columnar grains and a few equiaxed grains. The equiaxed grains, which at this location ranged from ASTM grain size 1 to 4, increased in number and degree of refinement with increasing proximity to the weld metal-base metal interface.

As a consequence of its location at the center of the weldment, bead 4 was subjected to thermal cycling twice, first from the deposition of bead 5 and again from the deposition of bead 3. This repeated thermal cycling resulted in a more refined structure which consisted mainly of equiaxed grains with very few columnar grains. The equiaxed grains in this area varied from ASTM grain size 3 to size 7 with the coarser grains, again, predominant near the fracture edge.

Fractography

Macroscopic examination of the fracture surface at the center of specimen A showed numerous small facets of varying orientation. These facets corresponded, in location, to the equiaxed grains in bead 4, as seen in the polished cross section (Fig. 3). The fracture mode in this area was largely intergranular (Fig. 5).

Although intergranular fracture was observed to some extent in the columnar and adjacent refined grain areas of each weld bead, as illustrated by Figs. 6 and 7, the fracture mode, as seen in Fig. 6, was generally transgranular. Both cleavage and microvoid coalescence (MVC) were found in the areas of transgranular fracture.

These findings agree substantially with those reported by Metzbower et al. [4] in their investigation of the relationship of fractography to macrostructure in SCC welds of HY-130 steel.

Hardness Measurements

Microhardness measurements showed a gradient in both the columnar grain zone and in the thermally cycled zone of each bead, the hardness increasing with increased distance from the fracture edge.

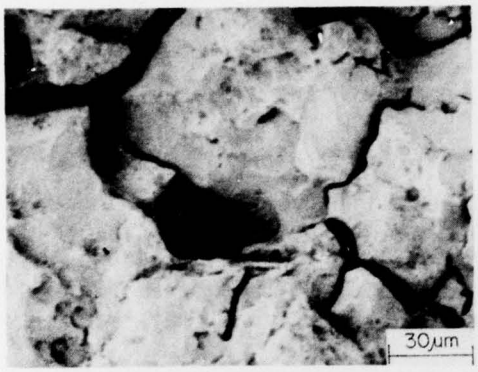

Fig. 5 — Intergranular fracture found in equiaxed grain area of weld bead 4

Fig. 6 — Columnar and adjacent refined grain areas showing predominantly transgranular fracture

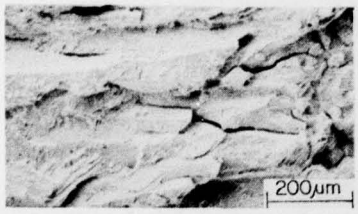

Fig. 7 — Intergranular fracture seen at the interface of the columnar and refined grain areas

Figure 8 is a plot of hardness and shows the variations with location in the columnar grain region of successive beads. Location A is approximately 100 microns (μm) from the fracture edge, and location E is approximately 100 μm from the weld metal–base metal interface. Locations B, C, and D are equidistantly spaced between A and E. Three measurements were made at each location and the values averaged. In Fig. 9 are plotted the results of similar measurements made in the thermally cycled zone of each successive weld bead.

Savage, Nippes, and Erickson [5], in an investigation of solidification mechanisms in fusion welds, and Davis and Garland [6], in reviewing the solidification structures and properties of fusion welds, point out that with the growth of columnar grains outward into the weld metal, the solute-rich liquid at the liquid-solid interface tends to be trapped at the weld centerline where the grains impinge. The result is the formation of a plane of weakness at the centerline with the possible impairment of the toughness of the weld deposit. Figure 3 shows the fracture to have propagated through the center of the columnar grain region of each bead, at the junction of the two solidification fronts. In bead 3, however, the fracture path deviated, propagating through an off-center grain and along the edge of the weld bead.

As seen from the data presented, the weld metal at the fracture edge, the path of crack propagation, was considerably softer than the remainder of the weldment. In general, these areas of relative softness coincided with the junction of the solidification fronts.

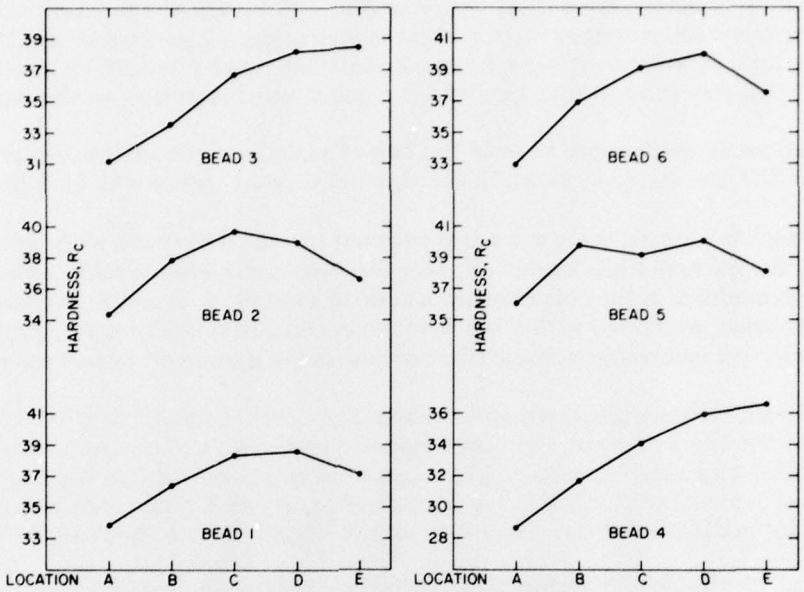

Fig. 8 — Variations in hardness with location in the columnar grain regions of successive weld beads

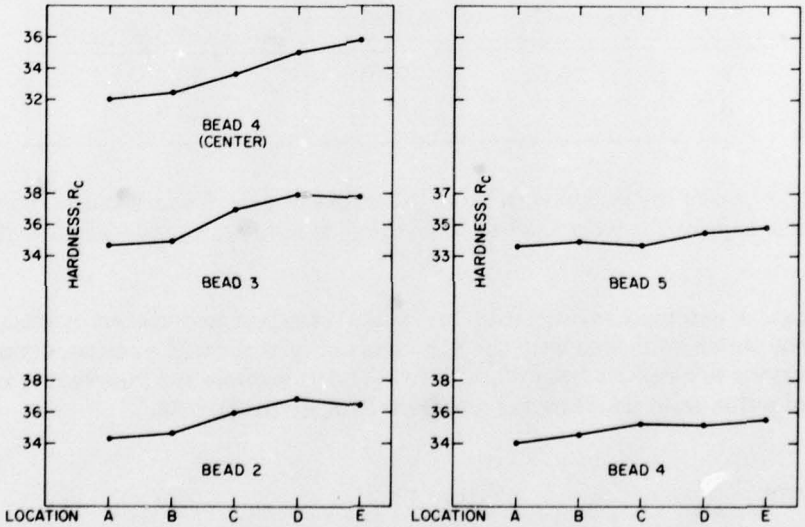

Fig. 9 — Variations in hardness with location in thermally cycled zones of successive weld beads

In bead 3, however, the softest area was found to be not the junction of the solidification fronts—the weld centerline—but a white etched zone, where further etching failed to resolve the microstructure. After surface contaminants were removed by sputtering, Auger analysis of this area showed that the carbon content was lower than in the adjacent areas.

The columnar grain zones showed the largest variations in hardness, ranging from 28.4 Rc to 40.0 Rc. The hardness range in the thermally cycled zones was 32.0 Rc to 38.0 Rc.

Although, in general, there was a trend toward increased hardness with increased distance from the fracture edge, location E, near the weld metal-base metal interface, showed a decrease in hardness in the columnar grain zone of beads 1, 2, 5, and 6. Microprobe analysis of these areas, which fell within the weld metal-base metal fusion zone, disclosed variations in chemical composition; these are discussed in the section on microsegregation.

Additional hardness measurements made at the extreme edge of weld bead 2 and weld bead 3 again showed a gradient, with the hardness increasing from the fracture edge toward the weld metal-base metal interface. These locations coincided with the light arcs seen in Fig. 2. Measurements were made at the fracture edge, the weld metal-base metal interface, and at a point midway between. The hardnesses obtained are listed in Table 2.

Table 2 — Hardness at Three Points in Beads 2 and 3

Bead	Hardness (Rc)		
	Fracture Edge	Midpoint	Weld Metal–Base Metal Interface
2	25.6	28.0	30.6
3	25.7	31.0	33.9

A comparison of these data with those presented in Figs. 8 and 9 shows the weld metal at the extreme edge of the weld bead to be a region of minimum hardness throughout the weldment.

Although an extensive investigation of the HAZ was not undertaken, it was noted that the base metal which coincided with the light arcs in Fig. 2 showed a coarse, equiaxed grain structure, varying in hardness from 33.0 Rc to 36.1 Rc, whereas the intervening areas were comprised of a fine grain structure varying from 37.8 Rc to 39.1 Rc.

Microstructure

The variations in hardness throughout the weld metal were reflected in the microstructure. The microstructure in the exact locations where the hardness measurements were taken has been illustrated, and the hardness at each indent has been indicated in order to show clearly the variations in these properties due to the range of cooling rates within a very small area of the weld bead. In the columnar grain areas, the microstructure ranged from auto-tempered martensite and fine granular bainite, found near the fracture edge (Fig. 10), to a

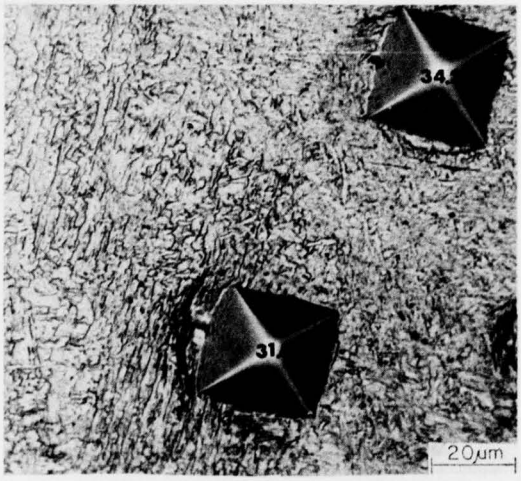

Fig. 10 — Microstructure—autotempered martensite and fine granular bainite—and hardness values (Rc) in columnar grain area near fracture edge (etched with 1% Nital)

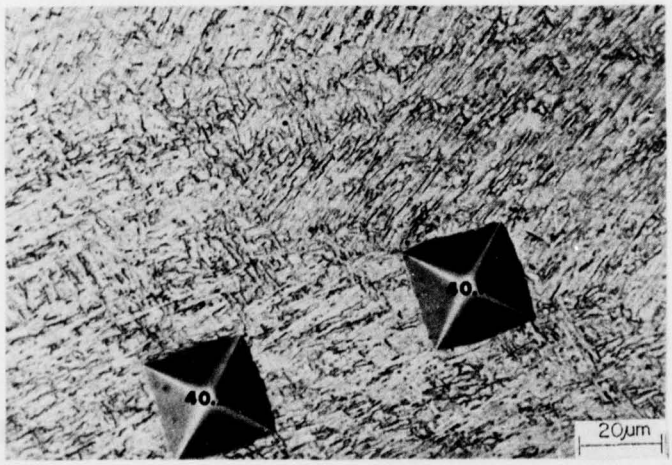

Fig. 11 — Microstructure and hardness (Rc) in columnar grain area near the fusion zone at the weld metal-base metal interface. The martensite showing relatively little tempering (etched with 1% Nital)

dark-etched untempered martensite located near the fusion zone at the weld metal-base metal interface (Fig.11). The dark-etched martensite coincided, in general, with location D of Fig. 8.

In the thermally cycled areas, highly tempered martensite and bainite (Fig. 12) or tempered martensite and acicular ferrite (Fig. 13) were the dominant microstructures.

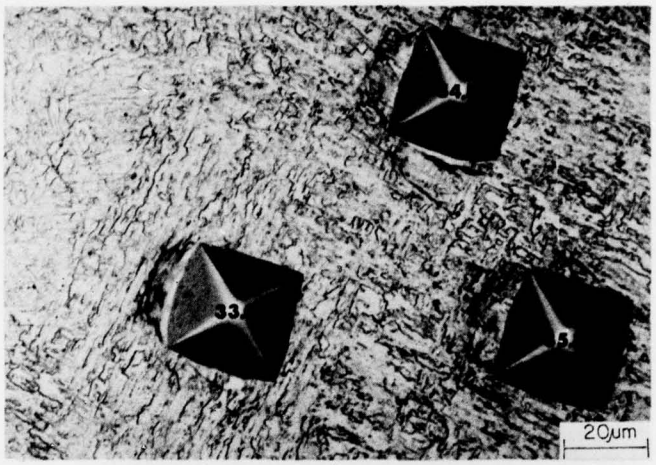

Fig. 12 — Microstructure—highly tempered martensite and bainite—and hardness (Rc) in the thermally cycled area (etched with 1% Nital)

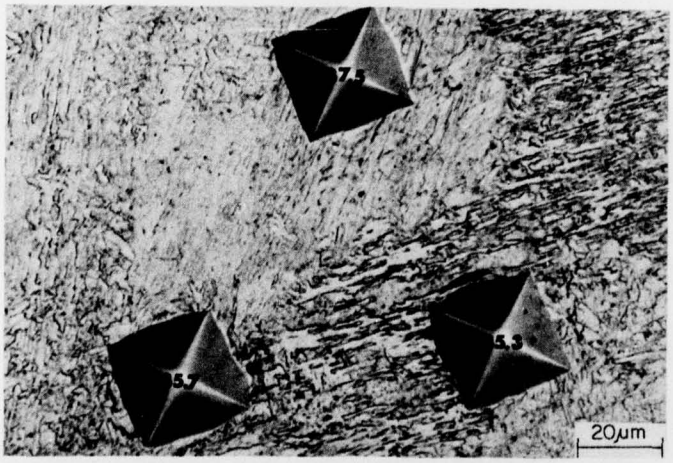

Fig. 13 — Microstructure—tempered martensite and acicular ferrite—and hardness (Rc) in the thermally cycled area (etched with 1% Nital)

The formation of bainite or acicular ferrite at the fracture edge (the weld bead centerline), is indicative of a slower cooling rate at the center of the weld pool. By contrast, the more rapid cooling which took place near the weld bead edge, in the vicinity of the weld metal-base metal interface, resulted in the formation of a martensitic microstructure which had been subjected to relatively little tempering.

Solidification Substructure

Savage, Lundin, and Aronson, in a study of fusion welds [7], concluded from the continuity of grains across the fusion boundary that solidification proceeds epitaxially

as the supercooled, molten weld metal wets the grains of unmelted base metal, of nominally the same composition, in the HAZ. Growth takes place from these grains into the weld pool.

An increase in under cooling and the redistribution of solute in the molten metal at the liquid/solid interface give rise to a range of solidification structures between the edge and the center of the weld bead. A predominantly cellular solidification mode was found in the weld metal adjacent to the base plate. With the build-up of a solute-rich layer in the liquid ahead of the liquid-solid interface, the solidification mode changed to a cellular-dendritic pattern. Evidence of solute rejection was found in the formation of pools of solute at the cell boundaries; the size and frequency of these pools increased with increased proximity to the weld bead centerline (Figs. 14 and 15).

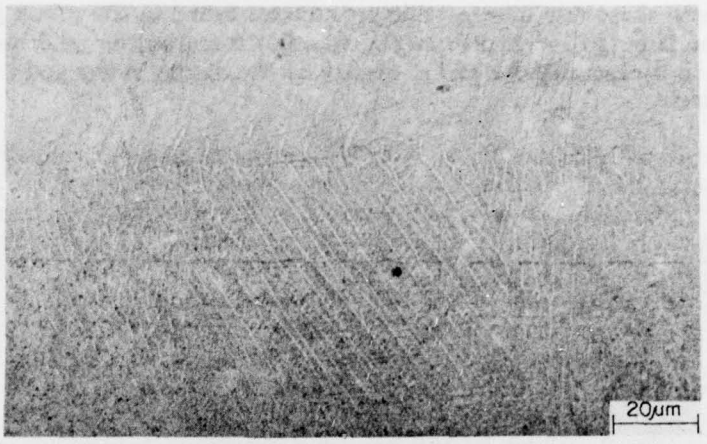

Fig. 14 — Solidification substructure near the weld metal-base metal interface showing small solute pools at the cell boundaries (etched with 10% ammonium persulfate solution)

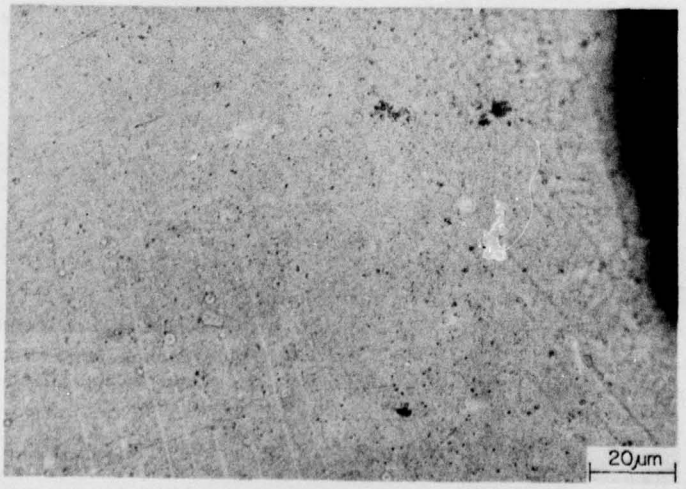

Fig. 15 — Solidification substructure near fracture edge showing relatively large solute pools at the cell boundaries (etched with 10% ammonium persulfate solution)

Segregation of Alloying Elements

X-ray microprobe analysis of the larger solute pools found at the fracture edge showed an increase in the concentration of the major alloying elements. These pools contained precipitates which in all likelihood were intermetallic compounds.

Where the precipitate was still present—that is, where it had not been removed during surface preparation prior to the analysis—a sharp increase in the x-ray count of the alloying elements, particularly Ni and Mn, was noted. In some instances, S was also detected.

In addition to these fine intermetallic precipitates found in the solute pools, a large metallic inclusion (Fig. 16), identified as Mo, was also found in the weld metal. Figures 17 and 18 show a backscattered electron display of the discontinuity and a Mo L_α x-ray display, respectively.

The backscattered electron display (Fig. 17) indicates an atomic number difference between the matrix and the included material; this display corresponds exactly to the morphology of the inclusion as seen at the center of the secondary electron display in Fig. 16. The x-ray display (Fig. 18) shows the distribution of Mo throughout.

Further inhomogeniety was seen in the weld metal fusion zone adjacent to the HAZ (Fig. 19). The line across the fusion zone indicates the path of the beam during microprobe analysis. Variations in the concentrations of the major alloying elements, Ni, Mn, and Cr, are shown in Fig. 20. Incomplete mixing of the filler metal and the melted base metal resulted in a zone of inhomogeniety which varied in width from 50 to 200 μm. Where location E (Fig. 8) fell within this zone, a decrease in hardness was noted.

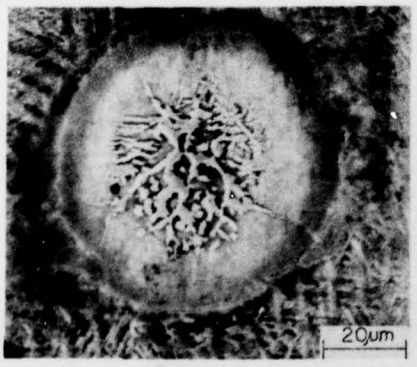

Fig. 16 — Mo inclusion (etched with 1% Nital)

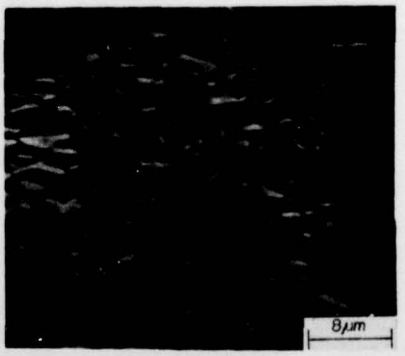

Fig. 17 — Backscattered electron display of the center of the inclusion seen in Fig. 16

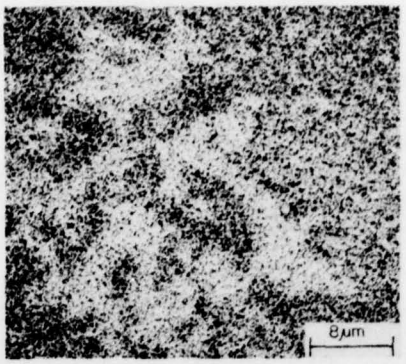

Fig. 18 — x-ray display showing distribution of Mo in the area of the inclusion seen in Fig. 17

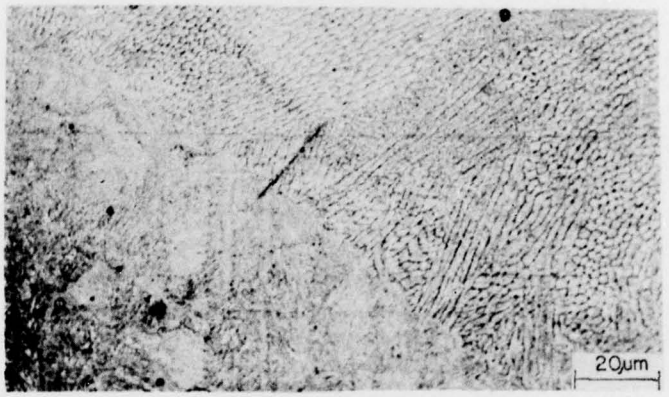

Fig. 19 — Weld metal fusion zone. Line indicates path of beam during microprobe analysis (etched with 10% ammonium persulfate solution).

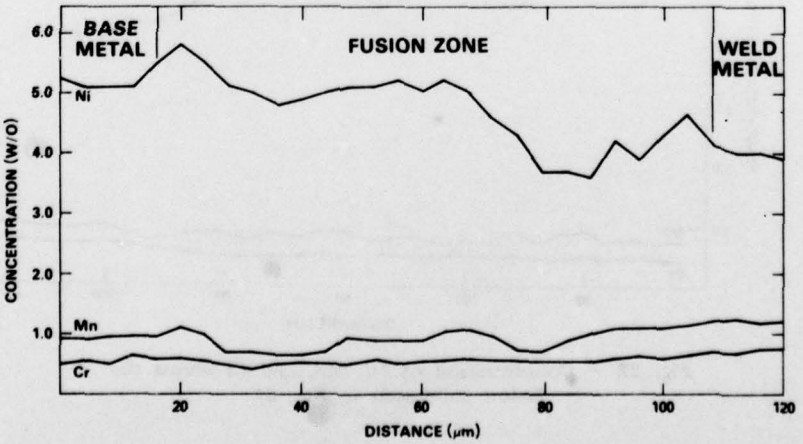

Fig. 20 — Variations in the concentration of Ni, Mn, and Cr across fusion zone seen in Fig. 19

As seen in Fig. 19, the fusion zone showed a dark etched band along the edge adjacent to the weld metal proper. However, at the center of the weldment, the fusion zone could not be readily identified optically (Fig. 21). Microprobe analysis of this area showed a more uniform compositional gradient (Fig. 22), suggesting more thorough mixing of the melted base metal and weld filler metal and the probable diffusion of the alloying elements due to the repeated thermal cycling at the root of the weldment.

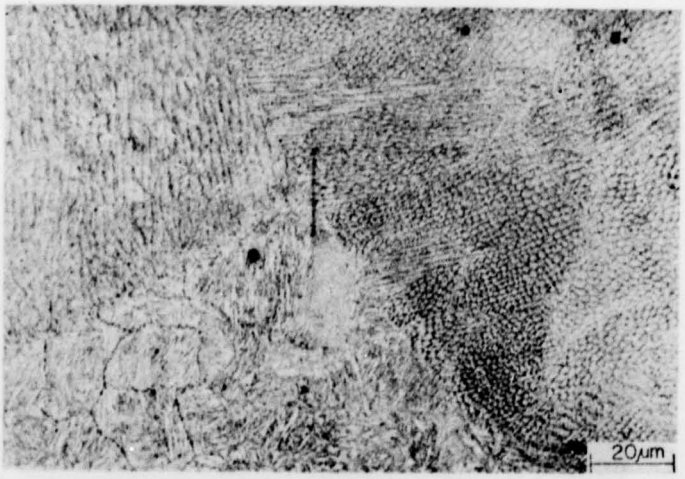

Fig. 21 — Fusion zone at the center of the weldment. Line indicates path of beam during microprobe analysis (etched with 10% ammonium persulfate solution).

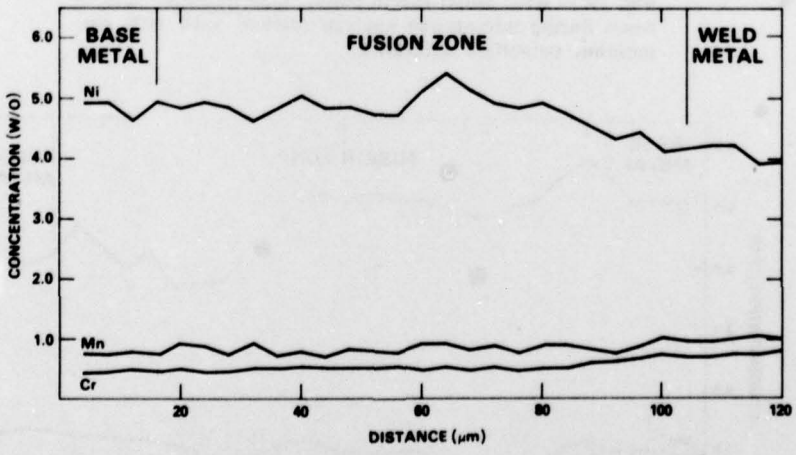

Fig. 22 — Concentration of Ni, Mn, and Cr across the fusion zone seen in Fig. 21

In a previous investigation [8] the fusion zones in a series of single and triple-pass, bead-on-plate weldments, including HY-130 (E14018) specimens, showed an unmixed zone (Fig. 23), comparable to that reported by Savage, Nippes, and Szerkeres [9] in their investigation of HY-80 steel weldments.

From the microprobe analysis (Fig. 24) it is clear that the dark etched zones in Fig. 23 are of weld metal composition, whereas the white areas within the solidification structure are of base metal composition; Fig. 23 indicates that virtually no mixing of the two metals had taken place. It appears that the extent to which mixing of the melted base metal and filler metal occurs or fails to occur, in the fusion zone, is due in some measure to the configuration of the base plate.

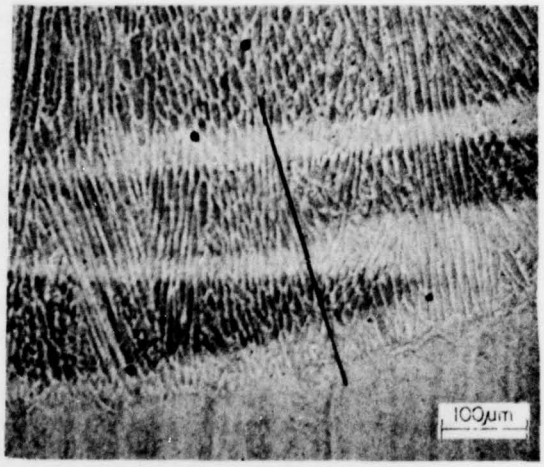

Fig. 23 — Unmixed fusion zone seen in HY-130 bead-on-plate weldment specimen. Line indicates path of beam during microprobe analysis (etched with *10% ammonium persulfate solution*).

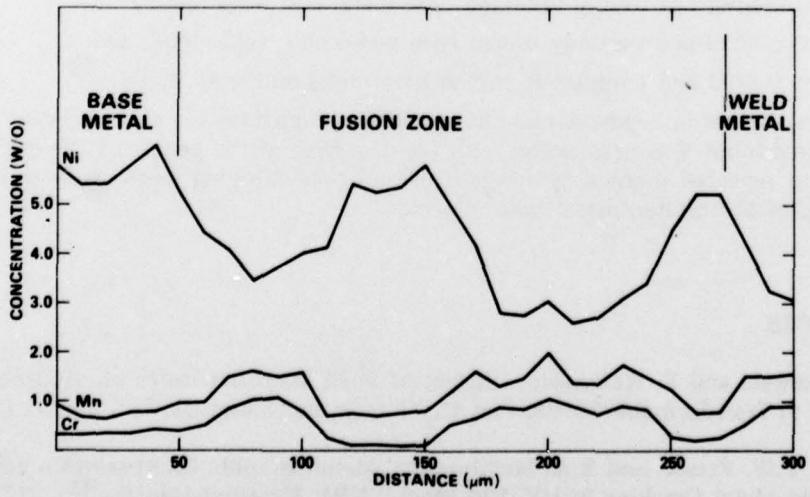

Fig. 24 — Variations in the concentration of Ni, Mn, and Cr across fusion zone seen in Fig. 23

Microprobe traces across the fusion boundaries between weld beads showed small variations in Mn content but no other segregation of alloying elements. Also, traces along and across the fracture edge in corresponding locations of sections A and B showed no recurring patterns of segregation.

CONCLUSIONS

1. In a SMA, multipass, double-V weldment, the most likely path of fracture is through the centers of the adjacent weld beads.

2. A hardness gradient exists within individual weld beads. The lowest values are found at the center of the bead and are reflected in the coarse grain size and in the microstructure, which is largely bainitic. Highest hardness values are found in the weld metal near the edge of the weld bead adjacent to the weld metal-base metal interface. At this location, the microstructure is martensitic and of a relatively fine grain structure.

3. As the solidification mode changes from cellular at the weld bead edge to cellular-dendritic at the center of the bead, microsegregation occurs in the form of pools of solute. These pools are a consequence of solute rejection due to increased supercooling at the liquid-solid interface, and they increase in size and number with increased proximity to the weld bead centerline. The concentration of the major alloying elements is higher in the solute pools than in the surrounding matrix.

4. Due to the configuration of the base plate, and to the degree of thermal cycling to which the weld metal has been subjected, the fusion zone in the weld metal adjacent to the HAZ can consist of;

   (a) melted but totally unmixed base metal and weld metal,

   (b) melted and partially mixed base metal and weld metal, and

   (c) melted and completely mixed base metal and weld metal.

Condition (a) occurs in bead-on-plate weldments. Conditions (b) and (c) occur in weldments of the double-V configuration with (c) occurring at the center of the double-V where, due to repeated thermal cycling, diffusion of the alloying elements as well as complete mixing of the molten metal takes place.

REFERENCES

1. T. Boniszewski and F. Watkinson, "Effect of Weld Microstructures on Hydrogen-Induced Cracking in Transformable Steels: Part II," Metals and Materials, 7, 145-151 (Mar. 1973).

2. J. Stoop, F.W. Fraser, and E.A. Metzbower, "Metallographic Interpretation and Analysis of Weld Metal Cracking in HY-130 Steel," NRL Memorandum Report 2777, Apr. 1974.

3. E.A. Metzbower and C.T. Fujii, "Stress Corrosion Cracking in HY-130/MIL-14018 Welds," NRL Memorandum Report 2820, June 1974.

4. E.A. Metzbower, C.T. Fujii, and J. Stoop, "Fractography as Related to Macrostructures in Stress Corrosion Cracked Welds in 5Ni-Cr-Mo Steel," pp. 62-74 in Fractography Microscopic Cracking Processes, ASTM, STP 600, American Society for Testing and Materials, Philadelphia, 1976.

5. W.F. Savage, E.F. Nippes, and J.S. Erickson, "Solidification Mechanisms in Fusion Welds," Welding J., Research Supplement 55, pp. 213-s to 221-s (Aug. 1976).

6. G.J. Davies and J.G. Garland, "Solidification Structure and Properties of Fusion Welds," International Metallurgical Reviews 20, 83-106 (1975).

7. W.F. Savage, C.D. Lundin, and A.H. Aronson, "Weld Metal Solidification Mechanics," Welding J., Research Supplement 44, pp. 175-s to 181-s (1965).

8. F.W. Fraser, "Segregation of Alloying Elements in Weld Metal", Report NRL Progress, May 1976, pp. 29-30.

9. W.F. Savage, E.F. Nippes, and E.S. Szekeres, "A Study of Weld Interface Phenomena in a Low Alloy Steel," Welding J., Research Supplement 55, 260-s to 268-s (Sept. 1976).